

# MULTIDISCIPLINARY DESIGN AND AERODYNAMIC ASSESSMENT OF AN AGILE AND HIGHLY SWEEPED AIRCRAFT CONFIGURATION

C. M. Liersch, K. C. Huber, A. Schütte  
German Aerospace Center, Institute of Aerodynamics and Flow Technology  
Braunschweig, Germany

D. Zimper  
German Aerospace Center, Program Coordination Defence and Security Research  
Cologne, Germany

M. Siggel  
German Aerospace Center, Simulation and Software Technology  
Cologne, Germany

## Abstract

The characteristics of highly swept aircraft configurations have been studied in a series of consecutive research projects in DLR for more than 15 years. Currently, the investigations focus on the generic SACCON UCAV configuration, which was specified in a common effort together with the NATO STO/AVT-161 task group. This paper is the first one in a series of articles presenting the SACCON-related research work within DLR. First, the article describes the conceptual design studies being performed for this aircraft configuration. At this point the question is raised, whether the simple aerodynamic methods used within conceptual design can be applied to such type of aircraft configurations with sufficient accuracy. Thus, the second part of this article provides a comparison of the aerodynamic characteristics of the SACCON configuration predicted by low- and high-fidelity aerodynamic methods, as well as some results from wind tunnel experiments.

## NOMENCLATURE

|           |   |   |
|-----------|---|---|
| $C_A$     | = | Axial force coefficient [-]             |
| $C_D$     | = | Drag force coefficient [-]              |
| $C_L$     | = | Lift force coefficient [-]              |
| $C_N$     | = | Normal force coefficient [-]            |
| $C_S$     | = | Body-fixed side force coefficient [-]   |
| $C_Y$     | = | Side force coefficient [-]              |
| $C_l$     | = | Rolling moment coefficient [-]          |
| $C_m$     | = | Pitching moment coefficient [-]         |
| $C_{mx}$  | = | Body-fixed X-moment coefficient [-]     |
| $C_{my}$  | = | Body-fixed Y-moment coefficient [-]     |
| $C_{mz}$  | = | Body-fixed Z-moment coefficient [-]     |
| $C_n$     | = | Yawing moment coefficient [-]           |
| $I_{xx}$  | = | Mass moment of inertia (X-axis) [-]     |
| $I_{yy}$  | = | Mass moment of inertia (Y-axis) [-]     |
| $I_{zz}$  | = | Mass moment of inertia (Z-axis) [-]     |
| $V$       | = | Freestream velocity [ $m/s$ ]           |
| $p, q, r$ | = | Rotation rates (X, Y, Z-axis) [ $1/s$ ] |

### Conventions

X, Y, Z = Coordinate system

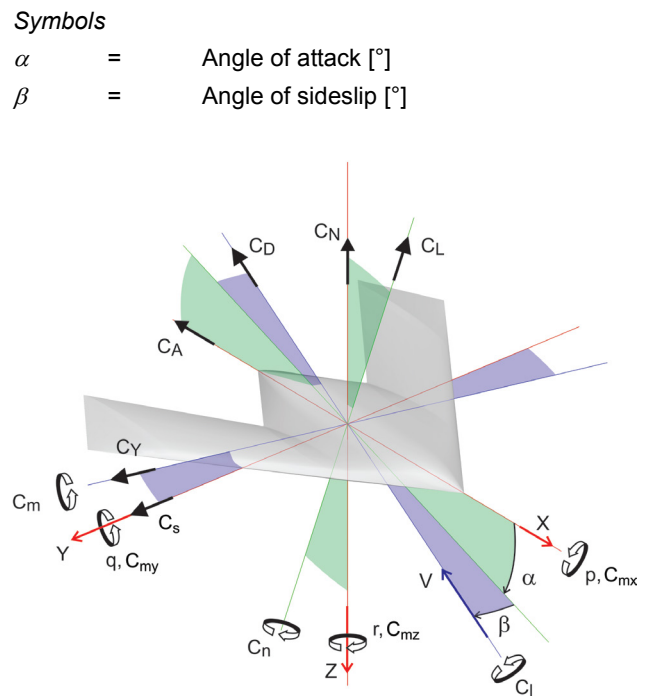


FIGURE 1. Coordinate System, see Vicroy et al. [1]

## 1. INTRODUCTION

Design and performance assessment of military aircraft configurations is an important topic for the German Aerospace Center (DLR<sup>1</sup>). In a series of consecutive projects, spanning over a period of more than 15 years, the characteristics of highly swept aircraft configurations have been investigated thoroughly (see FIGURE 2).

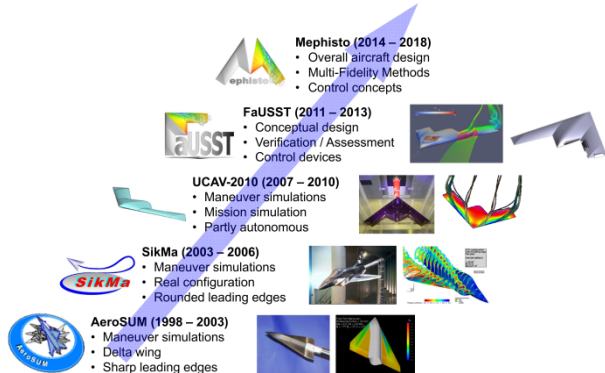


FIGURE 2. History of projects dealing with design and assessment of military aircraft configurations

Starting from a generic delta wing configuration featuring sharp leading edges, aerodynamic investigations including maneuver simulations were carried out within the project *AeroSUM*. For the subsequent project *SikMa*, the step towards a realistic and fully equipped fighter aircraft with rounded leading edges was made. At this point it turned out, that further investigations required a broader, more multi-disciplinary approach, including aircraft design capabilities. Hence, in the successor project *UCAV-2010*, a variety of different disciplines were joined for the design and assessment of a new, generic UCAV<sup>2</sup> configuration. Later, the basic design work for this UCAV configuration was extended by the *FaUSST* project emphasizing on stability and control aspects and linking the different disciplines together in conceptual aircraft design investigations. The current project *Mephisto*, focuses on the redesign of the UCAV shape from *UCAV-2010* with enhanced aerodynamic performance and concepts for control and propulsion as key aspects.

Since the days of *AeroSUM*, the understanding and the prediction capabilities of fighter type aircraft configurations have been considerably extended with respect to detailed flow physics, stability and control behavior, signatures, and aeroelastic characteristics. A variety of components, such as integrated air intakes and nozzles, the propulsion system, or the flight controller have been studied. Starting from *UCAV-2010*, a conceptual design process was built and used for overall aircraft design and assessment studies.

A detailed overview of the specific results from the various investigations performed within the DLR project *FaUSST*, as well as a perspective to its follow-on *Mephisto*, is provided in a series of articles, presented and published in the *DGLR<sup>3</sup> Deutscher Luft- und Raumfahrtkongress* in September 2015. While the papers by Huber et al. [2],

Schütte et al. [3], and Paul et al. [4] focus on aerodynamics, those by Nauroz [5] and Koch et al. [6] are emphasizing on propulsion and air intake aspects. The one by Voß [7] describes design and sizing of a structural model. Signature investigations are presented in the articles by Lindermeir [8] and Kemptner [9]. Finally, the papers by Schwithal et al. [10] and Kuchar et al. [11] are dealing with flight mechanics assessment and controller development.

This article covers two main topics: The first topic (see chapter 2) focuses on the conceptual UCAV design system, as well as on its application to the before mentioned UCAV configuration. In the second topic (see chapter 3), a series of aerodynamic studies is presented. The aim of these studies is to assess the usability of typical conceptual design aerodynamic tools for such a UCAV configuration.

## 2. CONCEPTUAL UCAV DESIGN

The first part of this article is dedicated to conceptual UCAV design. This is an essential capability for DLR, as the development of novel concepts and technologies has to incorporate an assessment of these in the context of a complete aircraft. Furthermore, in order to come to a realistic evaluation of the emerging advantages and drawbacks, this complete aircraft has to be optimized such as to exploit the new concept or technology up to a maximum. In section 2.1, the core concept of the applied design system is presented; section 2.2 provides an overview of the design work being performed for the UCAV concept being introduced in project *UCAV-2010*.

### 2.1. Design system

Aircraft design is a highly multidisciplinary task, involving experts from a number of disciplines such as aerodynamics, propulsion, structures, and many others. Even in the early stages of conceptual design it is very useful to have all these experts in the loop. This may help to avoid decisions which may later prove as problematic when looking more into detail. Especially the discipline of flight mechanics is often introduced at later stages of design since required data regarding aerodynamics, masses, and control surface efficiencies may not be available before. This late-binding of such a crucial discipline has led to a number of substantial problems during the history of aircraft design and should be prevented by providing comprehensive aircraft data as early as possible. Another advantage of early including disciplinary experts and their physics-based tools into the design process becomes apparent when designing unconventional aircraft configurations such as a highly swept flying wing UCAV. In this case, empirical handbook methods might lead to wrong results if the statistical basis from which they were derived does not cover the designed configuration sufficiently.

The concept to include disciplinary experts, their tools and knowledge even in the very beginning of the design process is one of the core concepts of the aircraft design system being developed by DLR since 2005 [12], [13], [14]. The system consists of three parts:

<sup>1</sup> Deutsches Zentrum für Luft- und Raumfahrt e.V.

<sup>2</sup> Unmanned Combat Air Vehicle

<sup>3</sup> Deutsche Gesellschaft für Luft- und Raumfahrt – Lilienthal-Oberth e.V.

- **Data exchange**

A data exchange file format called CPACS<sup>4</sup> is being developed for the DLR aircraft design system [15]. CPACS is an XML based data format which is designed to store aircraft data and geometries in a hierarchical and parametric way. It was introduced mainly to serve as a common language between the disciplinary analysis tools. Two software libraries [16] called TiXI<sup>5</sup> and TiGL<sup>6</sup> are being developed to ease the use of CPACS. While TiXI provides a simple interface to create, read, modify, and write XML datasets such as CPACS, TiGL generates a 3D CAD<sup>7</sup> model of the aircraft from the parametric data and offers methods to query geometric data from this model. In addition, TiGL provides functions to store the generated geometry to disk using standard CAD exchange file formats. The TiGL viewer application can be used to visualize the underlying CAD model. The complete package of CPACS and libraries is available under open source licenses [17], [18], [19].

- **Disciplinary analysis tools**

The analysis of an aircraft configuration is performed by disciplinary analysis tools which are provided and maintained by the disciplinary experts. For many disciplines, there is already more than one tool available - each one covering a different level of fidelity or using a different way of modeling. What they all have in common is the need to read and write CPACS datasets as input and output. For new tools, it is certainly a good way to use the CPACS data format directly. For legacy codes, which typically have (and shall keep) their own data formats, the best way is to use a so called "toolwrapper". A toolwrapper is a small program which reads a CPACS file, writes an input file for the tool, runs the tool, reads the output file of the tool and finally writes the results as a CPACS file. In order to keep the disciplinary experts in the loop and to avoid a decoupling of the used tools from further development, the tools are not gathered at one location to form a monolithic program. Instead, they are placed on disciplinary tool servers which stay under maintenance and supervision of the corresponding experts. Using a software integration framework, these distributed tools can be plugged together to form process chains for aircraft design and analysis.

- **Integration framework**

The software integration framework serves as a sort of construction kit. Here, the disciplinary tools, which are located on distributed servers, can be linked together to create process chains, customized for individual design or analysis tasks. Trade-study tools, different optimizers and other drivers of the process may be applied to get an impression of the sensitivities of the design parameters as well as optimal solutions for specific target functions. Up to now, the

commercial ModelCenter framework [20] was mainly used for this task, but will be replaced by the DLR integration framework RCE<sup>8</sup> in the future [21]. Just as CPACS, TiXI, and TiGL, RCE is provided under an open source license [22].

This aircraft design system was initially developed for the investigation of commercial transport aircraft. Within the projects *UCAV-2010* and *FaUSST*, it was extended and used for the investigation of a highly swept flying wing UCAV configuration

## 2.2. UCAV Design

With the aim of having a common, generic UCAV concept for research purposes, a new aircraft configuration was introduced in project *UCAV-2010*. While the basic, lambda shaped topology of this UCAV configuration was oriented towards the typical aim of low observability in combination with high agility, its details were specified in a way such as to have a geometry which could exactly be reproduced in a wind tunnel model as well as in a CFD<sup>9</sup> mesh. Another design aspect was to have a challenging aerodynamic behavior. This was reached by varying the leading edge over wingspan from sharp to round and back to sharp. The design of this, so-called "SACCON"<sup>10</sup> shape (see FIGURE 3), was carried out in a common effort with the NATO STO/AVT<sup>11</sup>-161 task group [23]. The original SACCON geometry has a wingspan of approx. 1.54 m which is well suited to build a wind tunnel model from it. The conceptual design task, presented in this article, was to develop a realistic UCAV concept based upon the original SACCON outer shape. This means, that it was only permitted to scale the whole SACCON geometry to a suitable size and to cut out parts for integrating components like control surfaces or engine inlets and nozzles.

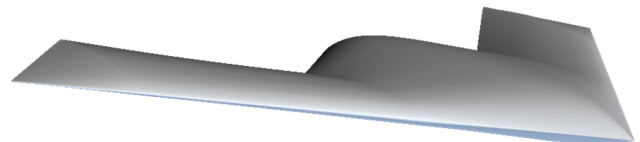


FIGURE 3. SACCON outer shape

In general, each aircraft is designed to fulfil one or more specific design missions. In this context, such a design mission incorporates a payload to be carried and a simplified flight trajectory (consisting at least of altitude and Mach number for a sequence of waypoints). Aside from the mission itself, an aircraft has to meet a number of further boundary conditions like operational requirements and certification rules. For this conceptual design study, only one design mission and a very limited number of additional boundary conditions were specified. The used boundary conditions are composed in TABLE 1. FIGURE 7 provides an overview of the design mission profile which was selected for the UCAV.

<sup>4</sup> Common Parametric Aircraft Configuration Schema

<sup>5</sup> TiXI XML Interface

<sup>6</sup> TiGL Geometry Library

<sup>7</sup> Computer Aided Design

<sup>8</sup> Remote Component Environment

<sup>9</sup> Computational Fluid Dynamics

<sup>10</sup> Stability And Control CONfiguration

<sup>11</sup> North Atlantic Treaty Organization  
Science and Technology Organization  
Applied Vehicle Technology

| Parameter          | Value                               |
|--------------------|-------------------------------------|
| Outer shape        | Scaled SACCON geometry              |
| Propulsion         | 1 or 2 turbofan engines             |
| Engine integration | Buried, due to signature reasons    |
| Payload storage    | internal (due to signature reasons) |
| Payload mass       | 1 × 2000 kg or 2 × 1000 kg          |
| Design range       | 3000 km (without refueling)         |
| Fuel reserve       | ≈ 45 min                            |
| Cruise altitude    | 11 km                               |
| Cruise Mach number | 0.8 (all altitudes)                 |
| Stability margin   | 2 – 8 %                             |

TABLE 1. Mission parameters and boundary conditions

The payload mass for the UCAV was defined to be 2000 kg in total. Due to signature requirements, an internal storage in one or two payload bays is mandatory. A design range of 3000 km without aerial refueling was considered sufficient – an extra reserve of approx. 45 minutes is desirable. With this assumption, an operational radius of 1500 km could be reached. Cruise flight to the target area shall be performed at an altitude of 11 km with a Mach number of 0.8. In the target area, the UCAV shall descend to an altitude of 300 m while keeping the Mach number of 0.8. During the last kilometers, it could even descend to 250 m and accelerate to Mach 0.9 – but due to the fixed outer shape, this is just an optional requirement. In order to keep a good maneuverability for this flying wing UCAV without making it laterally unstable, a stability margin of 2 – 8 % was selected. Based on these parameters, an initial estimation of the overall aircraft size and the corresponding take-off mass was made (see TABLE 2).

| Parameter                           | Initial | Final    |
|-------------------------------------|---------|----------|
| Scaling factor (compared to SACCON) | 8.0     | 10.0     |
| Wingspan                            | 12.3 m  | 15.375 m |
| Maximum take-off mass               | 10.0 t  | 15.0 t   |
| Thrust-to-weight ratio              | 0.35    | 0.4      |
| Static thrust                       | 35.0 kN | 60.0 kN  |

TABLE 2. Main aircraft parameters

These estimated values were used as a starting point for all further investigations and had to be updated during later stages of the design. Based on knowledge from conventional small fighter/trainer aircraft like the Northrop Grumman F5F Tiger II, the thrust-to-weight ratio was set to a relatively small value of 0.35, resulting in a required static thrust of 35 kN. Considering the fixed outer shape which is shown in FIGURE 4, a concept with a central payload bay and two engines aside would offer very limited vertical space for the engines, thus permitting only a low bypass ratio. Some preliminary studies showed that such a configuration would need a much larger scaling factor in order to store enough fuel to reach the specified design range. On the other hand, a single engine is more efficient by default and its location in the middle of the aircraft offers much more vertical space. Hence, this concept was chosen for further investigations. The payload bay was split into two parts which were placed on either side of the engine.

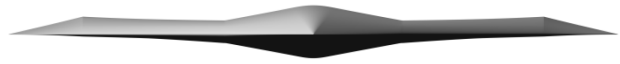


FIGURE 4. SACCON front view

After defining the starting point, the concept was investigated using the DLR conceptual design system. An engine with the required thrust and diameter was designed especially for this configuration and was included alongside the structural topology and other main components of the UCAV. Using the SACCON CAD geometry together with the already defined parameters, a CPACS model of the UCAV was created. This CPACS model, visualized by the TiGL-Viewer in FIGURE 5, was used as a central data repository being filled up during the design process. Furthermore, a Microsoft Excel spreadsheet with a 2D planform view of the geometry and its main components was created in order to calculate mass breakdown, center of gravity (CG), and mass moments of inertia. In order to be able to investigate changes in center of gravity locations and available fuel volume with respect to parameter changes, it was decided to integrate this spreadsheet directly into the process chain – even though it is limited to configurations which are quite similar to the current concept. In the future, a more common tool with similar features is expected to be available within the DLR design system.

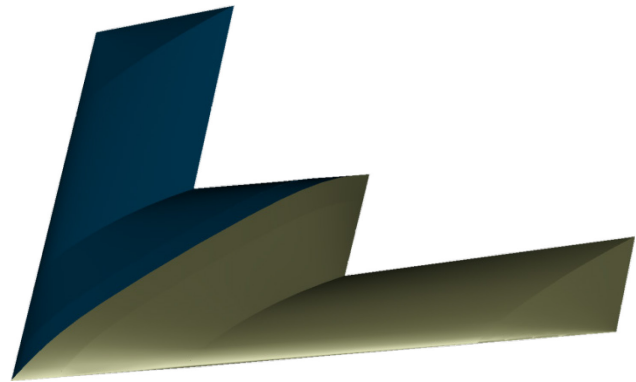


FIGURE 5. UCAV CPACS geometry model

FIGURE 8 illustrates the complete design process, as it was created for the UCAV design task: Starting from the CPACS source dataset (upper left corner), the workflow splits up into two main branches, which are computed in parallel, and a third branch (upper right corner). The latter is just responsible for visualizing the current geometry by using TiGL functionalities.

The first (left) one of the two branches creates a performance deck for the engine. This performance deck contains all relevant engine parameters (e.g. mass flows, temperatures, emissions) over a variety of flight levels, Mach numbers and thrust settings. The propulsion tool "TWdat" which is used here is a database, fed with a number of engines in advance. The engine design itself is performed separately in the gas turbine simulation environment [24]. The second branch (middle) creates a set of aerodynamic performance maps. The first set contains force and moment coefficients over a variety of Mach numbers, Reynolds numbers, angles of sideslip, and angles of attack for the "clean" configuration without control surface deflections. On top of this four-dimensional clean configuration dataset, a five-dimensional delta-coefficient performance map is created for each control surface (introducing the control surface deflection as fifth



dimension). By superposition of different control surface delta-coefficients with the absolute coefficients of the clean configuration dataset, it is possible to combine the deflections of multiple control surfaces. A third set of aerodynamic performance maps contains the damping derivatives for each point of the clean configuration dataset. Depending on the number of each of the dimensions' entries and on the number of control surfaces, this aerodynamic dataset may grow quite large. In fact, for the example presented here, it contains a number of 57 600 entries in total. Even with modern computer systems it is not possible to handle such a number of RANS<sup>12</sup>-CFD computations in an acceptable timeframe – but using simple, potential flow theory based aerodynamics methods, such a performance deck can be created within a few hours or even within minutes. In this process chain Analytical Methods' commercial "VSAERO" tool [25] is used in combination with DLR's simple "HandbookAero" method which accounts for skin friction drag and wave drag. Other tools, like DLR's open source "LIFTING\_LINE" method [26], [27], could be used here as a replacement for VSAERO as well. The question about the limitations of potential flow methods and whether they can be used to model such a configuration and the associated flow physics will be discussed in Chapter 3.

The results of the propulsion and aerodynamics branches are both joined together into the CPACS dataset and handed over to the "TotalMassCoG" script. Furthermore, the engine's mass and position are directly inserted into the Excel spreadsheet described above. The TotalMassCoG script imports mass data, center of gravity location and mass moments of inertia from this Excel spreadsheet and writes them into the CPACS as well. So at this point of the process chain, the dataset contains updated performance maps and total mass data. The following block is an iterative loop which calculates required fuel, landing gear mass, and structural mass. The left branch contains the tool "flightSimulation" which simulates a flight of the aircraft as specified in the design mission [28]. As a result, the flight trajectory and the required fuel are written back to the CPACS file. In the second branch, a script selects critical loadcases which are then calculated by the connected aerodynamic tools. Again, VSAERO and HandbookAero are used here, but in this case, the output of the aerodynamic tools is a number of spanwise distributions of the aerodynamic coefficients which can be used for structural sizing. In parallel to the first two branches, the right branch uses the tool "LGDesign" to analyze and size the landing gear [29]. As a result, it provides landing gear mass and critical ground loadcases which are combined with the spanwise aerodynamic coefficient distributions and fed as an input into the structural sizing tool "ModGen". ModGen creates a structural model of the UCAV and sizes the thicknesses of the elements [30]. The computed data for the UCAV's structural mass are combined with the fuel mass from the first branch to a resulting UCAV model. Finally the so-called "Converger" module checks, whether the resulting masses differ significantly from the ones used at start of the iteration loop, and, if necessary, it updates the Excel spreadsheet and starts the next iteration.

When the iteration finally has converged, a subsequent analysis process is started: In this case, the flightSimulation tool is used again, but this time it creates a

dynamic aircraft model which is handed over to the "HAREM" tool. HAREM is an analysis tool for investigating and evaluating the handling qualities of an aircraft [10], [31], [32].

The whole process chain was created using DLR's conceptual design system and runs completely automatically. In this case, it uses the ModelCenter integration framework for tool coupling and data exchange. Aside from small scripts and other supporting components it contains 7 different disciplinary tools (3 of them are even used twice in different working modes), residing on 6 servers, provided by 5 DLR Institutes, located at 4 different sites distributed over Germany.

As a result from running the process chain, it became obvious that the required fuel volume was nearly two times the available tank volume. Furthermore, it turned out that the payload bays would roughly need twice of the volume available and that the maximum take-off mass would significantly exceed the estimated amount of 10~metric~tons. As a consequence, the initially estimated parameters had to be revised: A second global scaling step – this time with a factor of 1.25 (meaning a factor of 10 compared to the SACCON geometry in total) and a new maximum take-off mass of 15 metric tons seemed promising here (see TABLE 2). After this resizing process, the engine had to be re-dimensioned as well. Taking this as an opportunity, the trust-to-weight ratio was also slightly increased to 0.4. The revised engine uses the extra space for a higher bypass ratio and provides increased thrust as required while showing a much lower specific fuel consumption. Main parameters of both engine designs are provided in TABLE 3 below.

| Parameter                 | Condition        | Unit           | Initial | Final   |
|---------------------------|------------------|----------------|---------|---------|
| Static thrust             | take-off         | <i>kN</i>      | 35.0    | 60.0    |
| Bypass ratio              | cruise<br>flight | –              | 1.56    | 3.78    |
| Overall pressure ratio    | take-off         | –              | 28.8    | 27.65   |
| Mass flow                 | take-off         | <i>kg/s</i>    | 60.8    | 149.05  |
| Turbine entry temperature | take-off         | <i>K</i>       | 1819.   | 1835.95 |
| Specific fuel consumption | cruise<br>flight | <i>g/(kNs)</i> | 22.82   | 20.03   |
| Fan diameter              | all              | <i>m</i>       | 0.65    | 1.12    |
| Length                    | all              | <i>m</i>       | 2.0     | 2.3     |
| Weight                    | all              | <i>kg</i>      | 700.0   | 1100.0  |

TABLE 3. Engine parameters

With this new aircraft size, the Excel spreadsheet was used to arrange the inner components in more detail so as to get the landing gear in the right place, to provide enough volume for fuel tanks and to find good locations for the other main components. The major task of this design step was to limit the longitudinal movement of the center of gravity in order to stay within the desired stability margins. Especially the highly swept fuel tanks with their

<sup>12</sup> Reynolds-Averaged Navier-Stokes equations

long lever arm and a fuel mass which is nearly half of the take-off mass caused problems. By introducing a second pair of fuel tanks far in front of the center of gravity and by cutting the rear outer parts of the wing tanks, this stability problem could finally be solved. Positioning the payload bays close to the center of gravity further reduced the movement of the aircraft's center of gravity. A snapshot of the UCAV's main components and center of gravity locations after their re-arrangement, but before starting the process chain is provided in FIGURE 9 (including "DETAIL-A"). During the process, the initially estimated masses are continuously changing until the iteration loop converges. After achieving convergence, the final center of gravity locations (take-off mass for design mission without reserve fuel) are shown in "DETAIL-B" of FIGURE 9.

One drawback of this Excel spreadsheet is that it does only contain a 2D model of the inner geometry, whereas the thickness of the UCAV varies continuously over the chord. As a consequence, it is not possible to determine from this model, whether a component really fits into the outer shape. As a solution to this problem, the spreadsheet was extended by a construction table for Dassault's CATIA CAD software [33]. Combined with an existing CAD model of the UCAV's outer shape, the CATIA software uses the construction table to generate the inner components as specified in the Excel spreadsheet. When the spreadsheet changes during the progress of the process chain, the corresponding CATIA model is updated automatically as well. The CATIA 3D model of the UCAV configuration with its main components is shown in FIGURE 6.

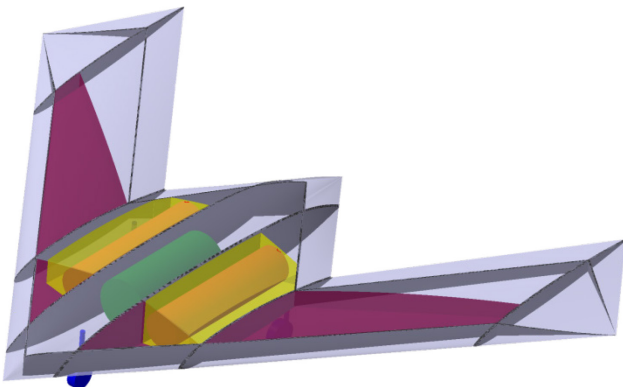


FIGURE 6. UCAV 3D view with inner components (CATIA)

A mass breakdown of the UCAV is provided in TABLE 4. It contains the masses of the main components, their center of gravity locations in X-direction and the mass moments of inertia for the main axis'. The deviation moments are currently neglected, as well as the center of gravity locations in Z-direction (set to zero). The table is taken from the Excel spreadsheet after running the process chain and shows the case of take-off mass with full payload bays and fuel for the design mission (but excluding reserve fuel). For this mission, the available fuel tank volume is used only by 84.4 %. Taking an average fuel burn per time over the complete mission, the remaining 15.6 % fuel volume ( $\approx 950$  kg) would equal to an additional flight time of approximately 37 minutes. If using the extra fuel to extend especially the high altitude cruise flight (which is the most efficient flight phase), the

additional flight time would increase to approximately 44 minutes. So the desired fuel reserve of about 45 minutes was finally met quite well. In the latter case, the take-off mass would increase to 15.15 metric tons, meeting the initially assumed 15.0 metric tons quite well, too.

The result from simulating the design mission with the final UCAV configuration is depicted in FIGURE 10. It shows altitude, angle of attack, Mach number and fuel flow over the mission duration and can be used to get a more detailed insight to the flight trajectory.

### 3. AERODYNAMIC ANALYSES

The conceptual design workflow described in the previous section needs an extensive amount of aerodynamic data for performance and load investigations. This database is currently created using simple and fast aerodynamic methods like VSAERO (used for the design study described in Section 2.2), or LIFTING\_LINE. VSAERO is a 3D singularity method based on the inviscid and incompressible potential flow theory, calculated on surface meshes. For investigating compressible flows, several compressibility corrections are included; viscous drag can optionally be considered through an iteratively coupled boundary layer module. LIFTING\_LINE is running faster than VSAERO, but is based on the even more simplified skeleton theory (also called camberline theory). In skeleton theory, the 3D surface is reduced to a set of flat panels; hence it neglects all effects coming from thickness. Further simplifications include a limitation to small angles of attack and sideslip. For compressible flows, LIFTING\_LINE offers a compressibility correction as well. Over the years, VSAERO and LIFTING\_LINE are well proven for investigating conventional transport aircraft configurations.

The question now is: How far can these simple methods be used for a highly swept flying wing aircraft? It is doubtless that the simple theory behind these tools is not able to model the complex vortex systems occurring for such aircraft, especially at higher angles of attack. On the other hand, this simple theory is known to behave conservatively in most cases. So the calculated loads are expected to be typically larger than what really will appear at the aircraft. On the other hand, this also means that control surface efficiencies might actually be much lower than predicted. In this Chapter, results from VSAERO and LIFTING\_LINE will be compared to measurements of the DLR-F19 wind tunnel model (which was built from the SACCON geometry) [34], [35], [36] and to RANS results created with the "DLR-TAU" code [37], [38], [39], [40]. The flow conditions for the comparison at subsonic speed are defined by the wind tunnel experiment: Mach number is 0.15, Reynolds number is  $1.6 \cdot 10^6$ , based on the DLR-F19 reference chordlength. For the comparison at transonic speeds real flight conditions of the initial full scale configuration have been considered (see TABLE 2, initial design with a scaling factor of 8): Mach numbers are 0.55, 0.8, 0.85, Reynolds number is  $23 \cdot 10^6$ .

TAU is a CFD tool developed by the DLR Institute of Aerodynamics and Flow Technology. It solves the compressible, three-dimensional, time-accurate RANS equations using a finite volume formulation. The code is based on a hybrid unstructured-grid approach, which

makes use of the advantages that prismatic grids offer in the resolution of viscous shear layers near walls, and the flexibility in grid generation offered by unstructured grids. The TAU computations for this study were performed using the SA<sup>13</sup> turbulence model at subsonic speed as well as at transonic speeds. Details about this model and the complete computational setup can be found in Schütte et al. [41] and Zimmer et al. [42]. As the LIFTING\_LINE computations are performed inviscid, the HandbookAero tool is applied afterwards in order to incorporate the turbulent viscous drag by using the method of the equivalent flat plate. For a better comparison, VSAERO is utilized twice here: Once using its own boundary layer module and once without that module, applying HandbookAero as it is done for LIFTING\_LINE. The computational meshes of the three aerodynamic methods are depicted in FIGURE 11, together with a picture of the DLR-F19 wind tunnel model.

Control surface deflections in LIFTING\_LINE and VSAERO are modeled just by rotating the normal vectors of the corresponding wing panels – but without changing the geometry itself. In LIFTING\_LINE, the hinge line for control surface deflection is always projected into the global Y-Z-Plane before use. This simplification of course leads to slightly different results, which will be discussed below. In the 3D TAU mesh (as well as in the wind tunnel model), the control surfaces are deflected geometrically, but without a gap. FIGURE 12 shows the control surface geometry used for LIFTING\_LINE and VSAERO (left) and for TAU and the wind tunnel model (right). On each side, there are two control surfaces: one inboard and one outboard. Regarding the side edges, the control surface definition used for LIFTING\_LINE and VSAERO is not able to model the geometry from the wind tunnel exactly. The simplification, which is currently used even leads to slightly bigger control surfaces and will certainly produce a small over-prediction of control surface effects.

### 3.1. Subsonic Speed

FIGURE 13 shows a comparison of the aerodynamic coefficients of the clean configuration for angles of attack from 0° up to 15°. As can be seen, the LIFTING\_LINE and VSAERO results generally do agree quite well. As expected, VSAERO VISCOUS exhibits a slightly lower lift curve slope due to the viscous effects and a far too low drag coefficient due to the fact that the computation was performed with free transition, resulting in a partial laminar boundary layer. For the pitching moment curves, they show a slight deviation, especially for higher angles of attack. However, since the moment reference point is located very close to the neutral point, the deviation only means a small discrepancy in the position of the neutral point and must not be overestimated. Compared to TAU and the experimental data, the lift curve shows a marginally higher slope (which is typical for potential flow theory) and a minimal shift in the zero-lift angle. The drag curve of the TAU results differs significantly from the experimental results. The reason for this deviation is the influence coming from the sting of the wind tunnel model. This was shown by a TAU simulation including the sting, performed by Schütte et al. [41]. For angles of attack up to 10°, the drag curves of LIFTING\_LINE and VSAERO are in good agreement with the TAU results; for higher angles

of attack, the drag is under-predicted by them, as the complex flow characteristics cannot be modeled sufficiently. In terms of pitching moment, there is again a strong deviation between TAU results and experimental data – especially for higher angles of attack. This effect is due to the experimental set up of the model: The belly sting arrangement of the wind tunnel contributes to the coefficient; the mounting is however not modeled in the computation. If modeled, improvements in coefficient prediction can be shown, see Schütte et al. [41]. In this case, a TAU computation with sting reduces the deviation and leads to similar gradients, but there is still an offset left between the two curves. As a reason for this offset, the article [41] suspects that the flow topology coming from the sting is not predicted correctly by TAU. Comparing the pitching moment curves from LIFTING\_LINE and VSAERO to the TAU results, it can be stated that they are in good agreement for low angles of attack. For angles of attack higher than 10° the discrepancy increases due to vortex effects which are not modeled by the simple methods. Finally, as it should be the case for a symmetrical geometry under symmetrical flow conditions, the side force coefficients are zero – as well as the rolling and yawing moment coefficients.

The effect of deflecting the control surfaces (left side upwards by 20°, right side downwards by 20°) is depicted as difference to the clean configuration (see FIGURE 13) in FIGURE 14. Generally, it can be stated that the effect on lift, drag, and pitching moment coming from control surface deflection is very small and in good agreement. The rolling moment coefficient offsets of TAU and experiment are nearly constant over the angle of attack and in very good agreement with each other. As expected, the results from VSAERO and LIFTING\_LINE are over-predicting this offset significantly. This effect is coming mainly from the 3D flow effects which are reducing the control surface efficiency and which are not modeled by the simple methods. The influence on the yawing moment is generally quite small. The trend of yawing moment development with increasing angle of attack is however represented correctly by all numerical methods considered. Here, LIFTING\_LINE over-predicts this development significantly, whereas VSAERO under-predicts it. Some small side force is existent in the experiments, which is predicted well by the TAU results. VSAERO increasingly over-predicts the side force with increasing angle of attack, though gives rise to the correct sign. One possibility, which will be further investigated in the future, could be that this effect is coming from mesh resolution and computational accuracy. LIFTING\_LINE here gives rise to a strongly over predicted side force, which is even of opposite sign. The reason for this effect is that the simple geometry model consisting of flat plates with a slight dihedral due to wing twist creates an unrealistic side force, being proportional to the angle of attack.

Looking at isolated control surface deflection cases, the same trends as for the combined deflections described above can be found. However, looking at higher angles of attack, the delta coefficients from TAU and experiment are not identical to the sum of isolated inboard and outboard delta coefficients. This means that the highly swept UCAV control surfaces are having a significant impact on each other due to 3D flow effects. Therefore, the combination of isolated control surface deflections by superposition of their delta coefficients – as commonly used for transport

<sup>13</sup>Spalart-Allmaras

aircraft with a lower wing sweep – is not sufficient for high angles of attack. LIFTING\_LINE and VSAERO are not predicting this cross-influence. Details about the differences between isolated and combined deflections are discussed by Liersch et al. [43].

In FIGURE 15 and FIGURE 16, the effects due to a sideslip variation are depicted. FIGURE 15 contains the total coefficients, whereas FIGURE 16 displays the deltas due to a combined control surface deflection (similar to the one used in FIGURE 14). In order to display the effects clearly, an angle of attack of  $10^\circ$  is chosen. The trends from VSAERO fit well to the results from TAU and from the wind tunnel measurements. The absolute values for the pitching moment are under-predicted; the rolling moment is significantly over-predicted. Taking into account that the absolute values are all quite low (except for the lift coefficient) the VSAERO results can be considered as sufficient, here. Regarding LIFTING\_LINE, it is obvious that there is nearly no influence from the sideslip angle. This effect is a result from the simplifications described above in combination with the SACCON geometry: Within LIFTING\_LINE, the SACCON geometry is nearly a totally flat plate. As the sideslip angle is considered to be small, the flow in X-direction is not reduced due to sideslip. Hence, the rolling moment coming from deflected control surfaces is slightly over-estimated and nearly independent from sideslip as well. On the other hand, the component from the incoming flow, which is oriented in Y-direction does not create significant effects because the LIFTING\_LINE geometry is nearly flat and the kinematic flow condition for each panel (including control surfaces) is evaluated in the X-Z-plane only. As a consequence, LIFTING\_LINE cannot predict the coefficients due to sideslip here.

### 3.2. Transonic Speeds

FIGURE 17, FIGURE 18, and FIGURE 19 show a comparison between LIFTING\_LINE, VSAERO and RANS results for a range of angles of attack between  $-5^\circ$  and  $15^\circ$  at Mach numbers of 0.55, 0.8, and 0.85. The RANS calculations were conducted with the initial design full-scale configuration without control surface deflections (see TABLE 2). For all Mach numbers a very good agreement can be seen comparing the results of the lift coefficients up to an angle of attack of  $10^\circ$ . As already indicated for the comparisons at subsonic speed, the nonlinear aerodynamic effects at higher angles of attack cannot be modeled by potential flow theory based methods like LIFTING\_LINE and VSAERO. Only the RANS computations are able to simulate the nonlinear vortex flow occurring at an angle of attack greater than  $10^\circ$ . A deviation can be seen between the pitching moment coefficient curves. A different gradient is indicated comparing the slope of the RANS curves with the LIFTING\_LINE and VSAERO curves. Taking into consideration the location of the neutral point with respect to the moment reference point, again, the deviation should not be overestimated. As expected, the nonlinear behavior for an angle of attack greater than  $10^\circ$  is not reflected by the LIFTING\_LINE and VSAERO curves. The drag coefficient is predicted quite well by LIFTING\_LINE and VSAERO. Due to the higher Mach and Reynolds numbers (compared to the low speed study in section 3.1), the laminar flow areas predicted by VSAERO VISCOUS are far smaller, thus resulting in a drag coefficient which is

very similar to the one computed using HandbookAero. Just for the combination of high Mach numbers and high angles of attack, the drag coefficients are becoming under-predicted.

FIGURE 20 shows the aerodynamic coefficients for sideslip angle sweeps at an angle of attack of  $6^\circ$ , a Mach number of 0.8, and a Reynolds number of  $23 \cdot 10^6$ . RANS results are compared again with LIFTING\_LINE and VSAERO results. The agreement between results for the lift, drag, and yawing moment coefficient can be stated as excellent. There is nearly no deviation between the different results. Additionally it can be seen, that an angle of sideslip of up to  $10^\circ$  has no remarkable influence on these three coefficients. With respect to the pitching moment coefficient, there are again significant deviations of LIFTING\_LINE and VSAERO from the TAU results, but as already mentioned for the results of the angle of attack investigations, the deviation should not be overestimated due to the location of the neutral point with respect to the moment reference point. Furthermore, VSAERO even predicts the slope of the moment curve quite well. Considering the side force coefficients, a good agreement between the different methods can be stated. The relative difference is quite big, but as the absolute values are very small, this is not considered as a problem here.

## 4. CONCLUSION

During a sequence of consecutive projects, the DLR conceptual design system was extended in order to permit design and analysis of highly swept flying wing UCAV configurations. A UCAV design task based on the generic SACCON geometry, specified together with the NATO STO/AVT-161 task group, was specified and a conceptual design workflow for this task was created. Together with partners from several disciplines, the UCAV design work was performed in a distributed process. A global scaling factor of 10 and an elaborated inner layout were the keys for fulfilling the design requirements. The question, whether simple and fast aerodynamic methods can provide suitable aerodynamic coefficients for such a configuration was investigated by comparison to RANS aerodynamics and wind tunnel measurements under low and high speed conditions. As a result, it can be stated that the coefficients from simple aerodynamic methods can be sufficient as long as the angles of attack are kept low. The effects of deflected control surfaces are typically covered with a slight overestimation, but are still sufficient for low angles of attack, as well. In case of transonic speeds in combination with high angles of attack, a suitable wave drag estimation could help to improve the accuracy of the computed drag coefficients. If an emphasis is placed on sideslip in combination with flat aircraft configurations, methods that are not neglecting the thickness have to be used. At higher angles of attack, especially the pitching moment from simple methods might develop strong deviations to reality, both in total values and trends. So, a mission analysis for fuel estimation can normally use coefficients from simple methods without problems. For the design of a flight control system or other flight dynamic investigations being performed in the early stages of design, aerodynamic data coming purely from simple methods might not be sufficient. In such cases, a multi-fidelity approach could help to correct thousands of potential flow computations by a few well selected RANS computations or wind tunnel measurements.



## 5. ACKNOWLEDGEMENT

The design work presented here was performed in close cooperation with DLR-colleagues from all involved disciplines, namely aeroelastics, flight mechanics and systems, infrared-signatures, propulsion, radar-signatures, structures, system dynamics and control. The authors would like to thank all colleagues who contributed to this design work. An additional acknowledgement has to be given to the community of the DLR conceptual design system.

## REFERENCES

- [1] Vicroy, D. D., Huber, K. C., Loeser, T., and Rohlf, D., "Low-speed Dynamic Wind Tunnel Test Analysis of a Generic 53° Swept UCAV Configuration with Controls", 32nd AIAA Applied Aerodynamics Conference, No. AIAA-2014-2003, Atlanta, GA, June 2014.
- [2] Huber, K., Rein, M., Schütte, A., and Löser, T., "Experimental Aerodynamic Assessment and Evaluation of an Agile Highly Swept Aircraft Configuration", DGLR, Deutscher Luft- und Raumfahrtkongress, Rostock, September 2015.
- [3] Schütte, A., Huber, K., and Zipper, D., "Numerische aerodynamische Analyse und Bewertung einer agilen und hoch gepfeilten Flugzeugkonfiguration", DGLR, Deutscher Luft- und Raumfahrtkongress, Rostock, September 2015.
- [4] Paul, M., Rütten, M., and Rein, M., "Numerische Untersuchungen von nicht konventionellen Steuerkonzepten für eine agile und hoch gepfeilte Flugzeugkonfiguration", DGLR, Deutscher Luft- und Raumfahrtkongress, Rostock, September 2015.
- [5] Nauroz, M., "Antriebskonzept einer agilen und hoch gepfeilten Flugzeugkonfiguration", DGLR, Deutscher Luft- und Raumfahrtkongress, Rostock, September 2015.
- [6] Koch, S., Rütten, M., and Rein, M., "Experimentelle und numerische Untersuchungen zu integrierten Einläufen für agile und hoch gepfeilte Flugzeugkonfigurationen", DGLR, Deutscher Luft- und Raumfahrtkongress, Rostock, September 2015.
- [7] Voß, A., "Design and Sizing of a Parametrized Structural Model for a UCAV Configuration for Loads and Aeroelastic Analysis", DGLR, Deutscher Luft- und Raumfahrtkongress, Rostock, September 2015.
- [8] Lindermeir, E. and Rütten, M., "Infrarotsignaturbewertung von agilen und hoch gepfeilten Flugzeugkonfigurationen", DGLR, Deutscher Luft- und Raumfahrtkongress, Rostock, September 2015.
- [9] Kemptner, E., "Radarsignaturbewertung von agilen und hoch gepfeilten Flugzeugkonfigurationen", DGLR, Deutscher Luft- und Raumfahrtkongress, Rostock, September 2015.
- [10] Schwithal, J., Rohlf, D., Looye, G., and Liersch, C. M., "An innovative route from wind tunnel experiments to flight dynamics analysis for highly swept flying wing", DGLR, Deutscher Luft- und Raumfahrtkongress, Rostock, September 2015.
- [11] Kuchar, R., Steinhäuser, R., and Looye, G., "Reglerentwurf für eine agile und hoch gepfeilte Flugzeugkonfiguration", DGLR, Deutscher Luft- und Raumfahrtkongress, Rostock, September 2015.
- [12] Liersch, C. M. and Hepperle, M., "A Unified Approach for Multidisciplinary Preliminary Aircraft Design", CEAS 2009 European Air and Space Conference, October 2009.
- [13] Liersch, C. M. and Hepperle, M., "A distributed toolbox for multidisciplinary preliminary aircraft design", CEAS Aeronautical Journal, Vol. 2, No. Number 1-4, December 2011, pp. 57{68.
- [14] Nagel, B., Zill, T., Moerland, E., and Böhnke, D., "Virtual Aircraft Multidisciplinary Analysis and Design Processes - Lessons Learned from the Collaborative Design Project VAMP", CEAS 2013 European Air and Space Conference, September 2013.
- [15] Nagel, B., Böhnke, D., Gollnick, V., Schmollgruber, P., Rizzi, A., Rocca, G. L., and Alonso, J. J., "Communication in Aircraft Design: Can we establish a Common Language?", 28th International Congress of the Aeronautical Sciences (ICAS), 2012.
- [16] Bachmann, A., Kunde, M., Litz, M., and Schreiber, A., "A dynamic data integration approach to build scientific work flow systems", International workshop on work flow management (IWM 2009), The institute of electrical and electronics engineers, Inc., May 2009, pp. 27-33.
- [17] "CPACS Homepage", URL: <http://software.dlr.de/p/cpacs/home/> [cited 31 August 2015].
- [18] "TiXI Homepage", URL: <http://software.dlr.de/p/tixi/home/> [cited 31 August 2015].
- [19] "TiGL Homepage", URL: <http://software.dlr.de/p/tigl/home/> [cited 31 August 2015].
- [20] "ModelCenter Homepage", URL: <http://www.phoenix-int.com/modelcenter/integrate.php> [cited 31 August 2015].
- [21] Seider, D., Fischer, P., Litz, M., Schreiber, A., and Gerndt, A., "Open Source Software Framework for Applications in Aeronautics and Space", IEEE Aerospace Conference, March 2012.
- [22] "RCE Homepage", URL: <http://software.dlr.de/p/rcenvironment/home/> [cited 31 August 2015].
- [23] Cummings, R. and Schütte, A., "An Integrated Computational/Experimental Approach to UCAV Stability & Control Estimations: Overview of NATO RTO AVT-161", 28th AIAA Applied Aerodynamics Conference, No. AIAA-2010-4392, 2010.
- [24] Becker, R.-G., Wolters, F., Nauroz, M., and Otten, T., "Development of a Gas Turbine Performance Code and its Application to Preliminary Engine Design", DLRK 2011, September 2011.
- [25] "VSAERO Homepage", URL: <http://www.ami.aero/software-computing/ami-computational-fluid-dynamics-tools/vsaero/> [cited 31 August 2015].
- [26] Horstmann, K. H., "Ein Mehrfach-Traglinienverfahren und seine Verwendung für Entwurf und Nachrechnung nichtplanarer Flügelanordnungen", Tech. rep., Deutsche Forschungs- und Versuchsanstalt für Luft- und Raumfahrt, 1987.
- [27] Liersch, C. M. and Wunderlich, T. F., "A Fast Aerodynamic Tool for Preliminary Aircraft Design", 12th AIAA / ISSMO Multidisciplinary Analysis and Optimization Conference, No. AIAA-2008-5901, September 2008.

- [28] Looye, G., "TECS/THCS-based generic autopilot control laws for aircraft mission simulation", Second CEAS Specialist Conference on Guidance, Navigation and Control, June 2013.
- [29] Krüger, W., Cumnuantip, S., and Liersch, C., "Multidisciplinary Conceptual Design of a UCAV Configuration", RTO/AVT Panel Workshop "Virtual Prototyping of Affordable Military Vehicles Using Advanced MDO", 2011.
- [30] Klimmek, T., "Parameterization of Topology and Geometry for the Multidisciplinary Optimization of Wing Structures", CEAS 2009 European Air and Space Conference, October 2009.
- [31] Duus, G. and Duda, H., "HAREM - HANDling Qualities Research and Evaluation using Matlab", IEEE International Symposium on Computer Aided Control System Design, Kohala Coast, HI (us), 22-27 August 1999, 1999, pp. 428{432.
- [32] Ehlers, J., "Flying Qualities Analysis of CPACS Based Aircraft Models - HAREM V2.0 -", Tech. rep., German Aerospace Center (DLR), Institute for Flight Systems, June 2013.
- [33] "CATIA Homepage", URL: <http://www.3ds.com/de/produkte-und-services/catia/> [cited 31 August 2015].
- [34] Löser, T., Vicroy, D., and Schütte, A., "SACCON Static Wind Tunnel Tests at DNW-NWB and 14'x22' NASA LaRC", 28th AIAA Applied Aerodynamics Conference, No. AIAA-2010-4393, 2010.
- [35] Vicroy, D. D., Loeser, T. D., and Schütte, A., "Static and Forced-Oscillation Tests of a Generic Unmanned Combat Air Vehicle", Journal of Aircraft, Vol. Volume 49, No. 6, November 2012, pp. 1558{1583.
- [36] Huber, K. C., Vicroy, D., Schütte, A., and Hübner, A. R., "UCAV model design and static experimental investigations to estimate control device effectiveness and Stability and Control capabilities", 32nd AIAA Applied Aerodynamics Conference, No. AIAA-2014-2002, Atlanta, GA, June 2014.
- [37] Galle, M., Gerhold, T., and Evans, J., "Technical Documentation of the DLR TAU-Code", Tech. Rep. DLR-IB 233-97/A43, DLR, 1997.
- [38] Gerhold, T., Friedrich, O., Evans, J., and Galle, M., "Calculation of Complex Three-Dimensional Configurations Employing the DLR-tau-Code", 35th Aerospace Sciences Meeting & Exhibit, January 6-10, 1997, Reno, NV, No. AIAA-1997-0167, January 1997.
- [39] Gerhold, T., "Overview of the Hybrid RANS Code TAU", Closing Presentation DLR Project MEGAFLOW, Braunschweig (de), 10.-11.12.2002, edited by N. Kroll and J. Faßbender, Vol. 89 of Notes on Numerical Fluid Mechanics and Multidisciplinary Design (NNFM), Springer Verlag, 2005.
- [40] Schwamborn, D., Gerhold, T., and Heinrich, R., "The DLR TAU-Code: Recent Applications in Research And Industry", ECCOMAS CFD 2006 Conference, 2006.
- [41] Schütte, A., Huber, K. C., and Boelens, O. J., "Static and dynamic numerical simulations of a generic UCAV configuration with and without control devices", 32nd AIAA Applied Aerodynamics Conference, No. AIAA-2014-2132, Atlanta, GA, June 2014.
- [42] Zimper, D., Hummel, D., "Analysis of the transonic flow around a generic UCAV configuration", 32nd AIAA Applied Aerodynamics Conference, No. AIAA-Paper 2014-2266, Atlanta, GA, June 2014.
- [43] Liersch, C. M., Huber, K. C., "Conceptual Design and Aerodynamic Analyses of a Generic UCAV Configuration", 32nd AIAA Applied Aerodynamics Conference, No. AIAA-Paper 2014-2001, Atlanta, GA, June 2014.

## APPENDIX

| Component            | Mass [kg]     | CG Coordinates |             |             | Mass Moments of Inertia (CG)        |                                     |                                     |
|----------------------|---------------|----------------|-------------|-------------|-------------------------------------|-------------------------------------|-------------------------------------|
|                      |               | X [m]          | Y [m]       | Z [m]       | I <sub>xx</sub> [kgm <sup>2</sup> ] | I <sub>yy</sub> [kgm <sup>2</sup> ] | I <sub>zz</sub> [kgm <sup>2</sup> ] |
| Structures           | 2 677         | 6.33           | 0.00        | 0.00        | 30 486                              | 3 436                               | 33 922                              |
| Landing Gear         | 496           | 5.63           | 0.00        | 0.00        | 1 514                               | 1 441                               | 2 955                               |
| Propulsion           | 1 541         | 5.40           | 0.00        | 0.00        | 0                                   | 677                                 | 677                                 |
| Systems              | 1 790         | 4.65           | 0.00        | 0.00        | 0                                   | 7 627                               | 7 627                               |
| Other                | 559           | 5.42           | 0.00        | 0.00        | 760                                 | 23                                  | 783                                 |
| <b>Empty Mass</b>    | <b>7 062</b>  | <b>5.58</b>    | <b>0.00</b> | <b>0.00</b> | <b>32 760</b>                       | <b>13 204</b>                       | <b>45 964</b>                       |
| Payload              | 2 000         | 5.40           | 0.00        | 0.00        | 3 380                               | 62                                  | 3 442                               |
| <b>Forward CG</b>    | <b>9 092</b>  | <b>5.54</b>    | <b>0.00</b> | <b>0.00</b> | <b>36 140</b>                       | <b>13 267</b>                       | <b>49 407</b>                       |
| Fuel                 | 5 140         | 5.64           | 0.00        | 0.00        | 58 498                              | 19 350                              | 77 849                              |
| <b>Rearward CG</b>   | <b>12 202</b> | <b>5.61</b>    | <b>0.00</b> | <b>0.00</b> | <b>91 258</b>                       | <b>32 555</b>                       | <b>123 813</b>                      |
| <b>Take-off mass</b> | <b>14 202</b> | <b>5.58</b>    | <b>0.00</b> | <b>0.00</b> | <b>94 638</b>                       | <b>32 617</b>                       | <b>127 255</b>                      |

TABLE 4. Mass, CG location, and mass moments of inertia around CG

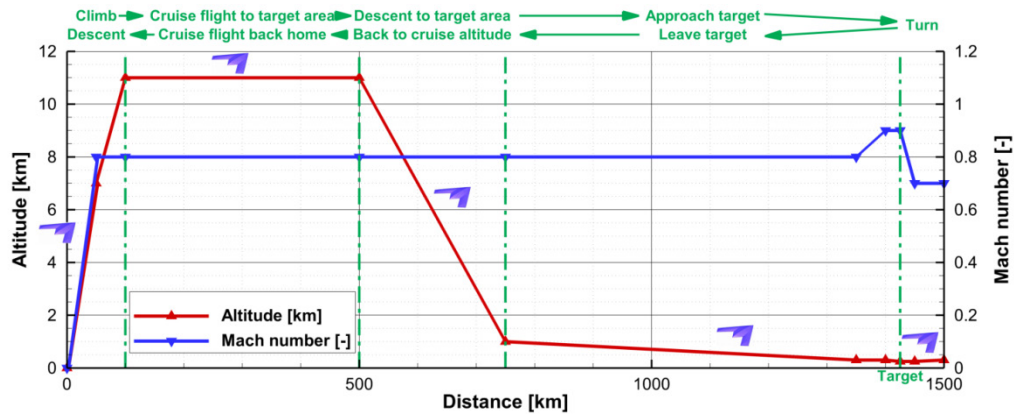


FIGURE 7. UCAV design mission

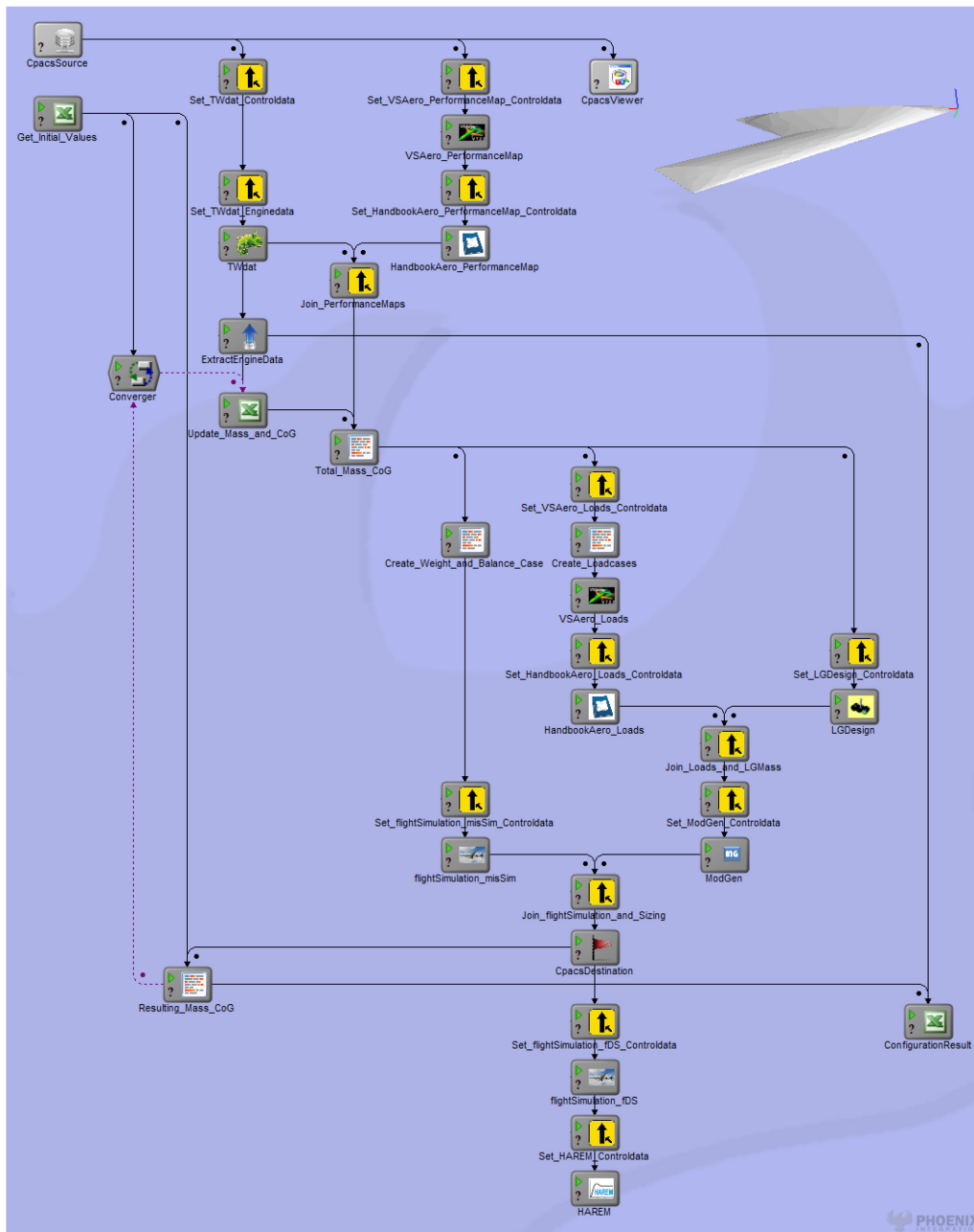


FIGURE 8. Conceptual design process (ModelCenter)

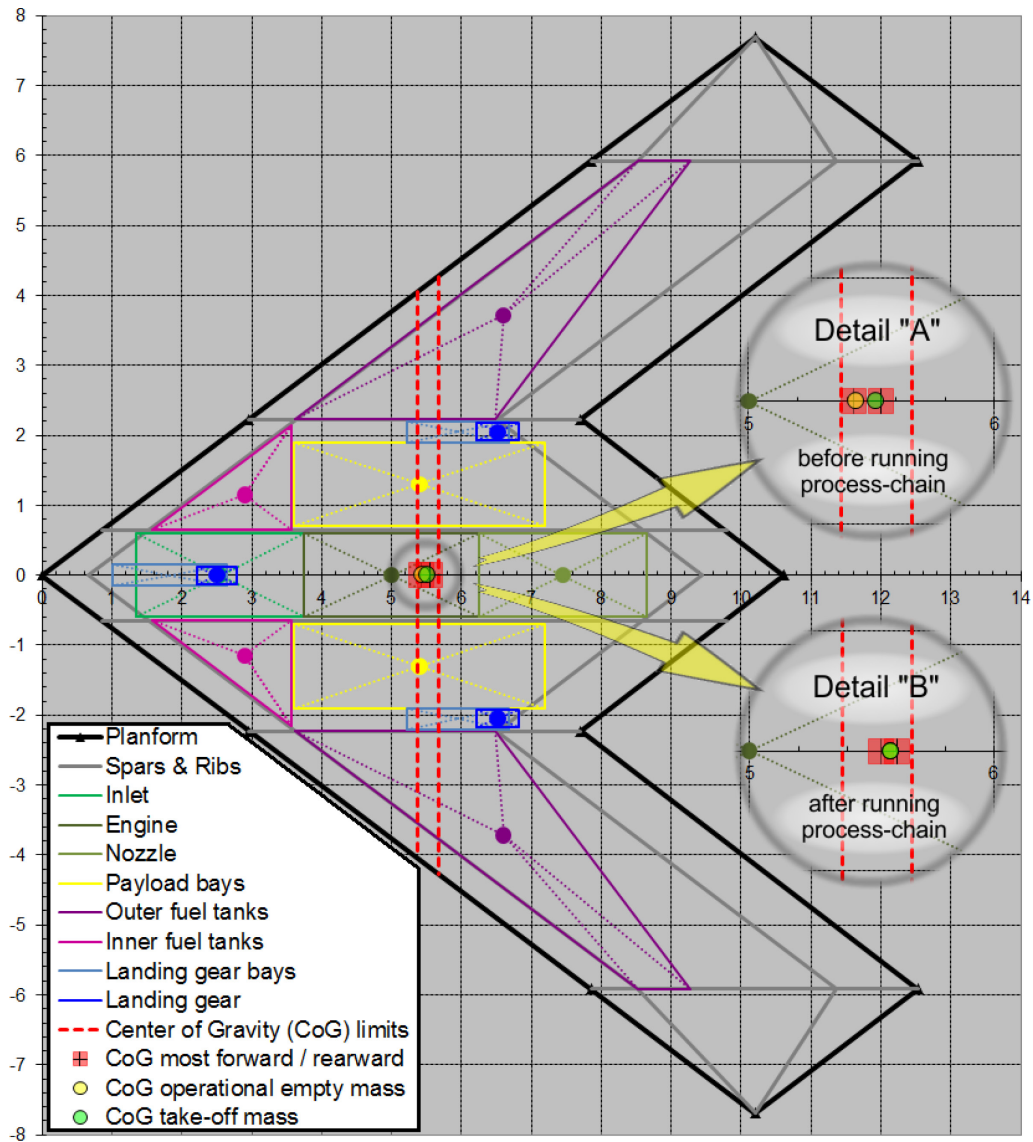


FIGURE 9. Main components of the UCAV configuration

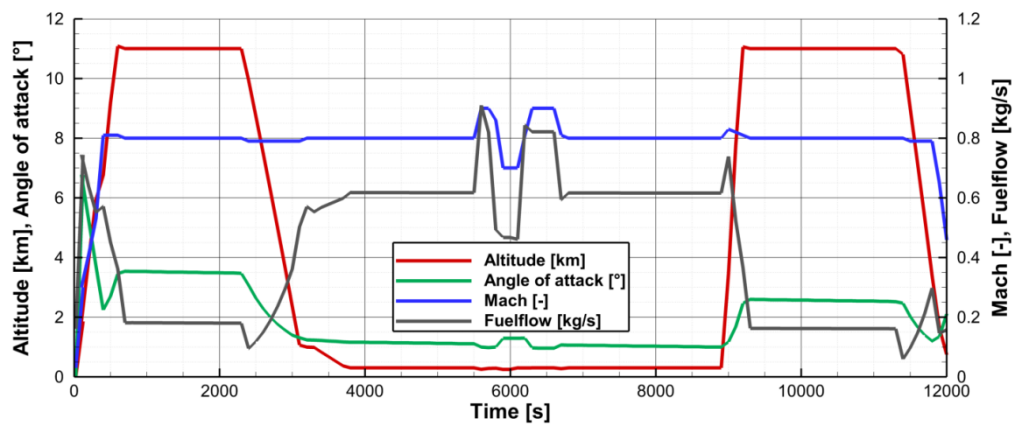
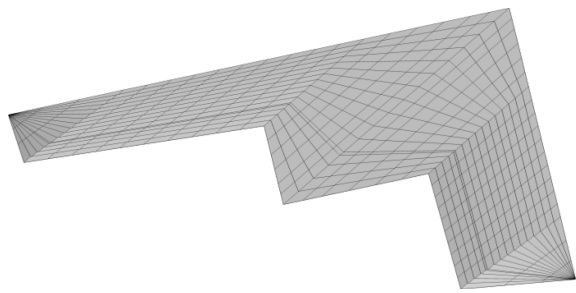
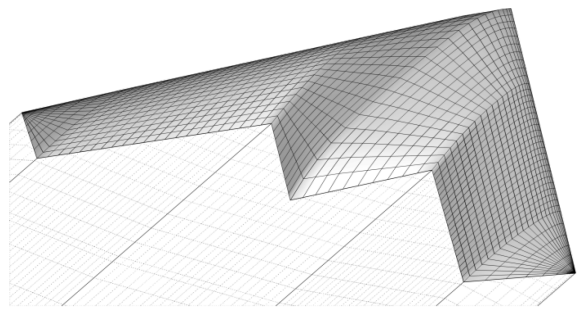


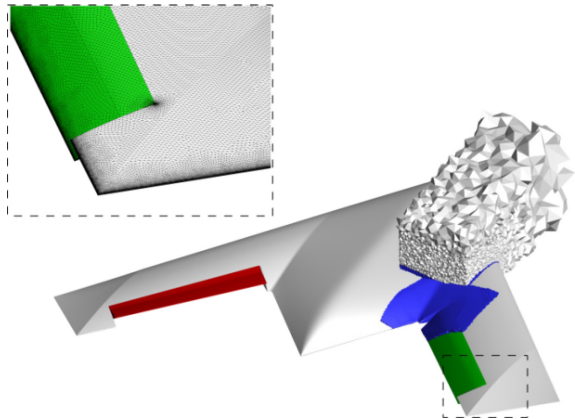
FIGURE 10. Trajectory of the simulated design mission



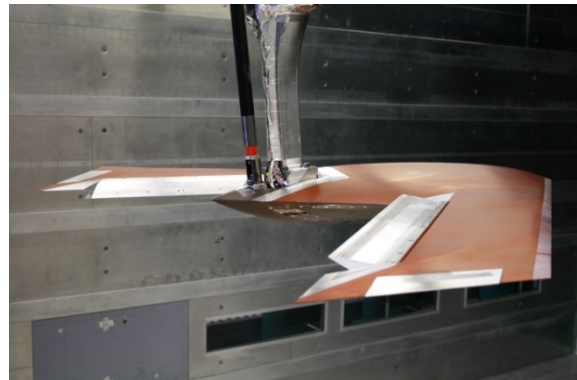
(a) LIFTING\_LINE mesh



(b) VSAERO mesh

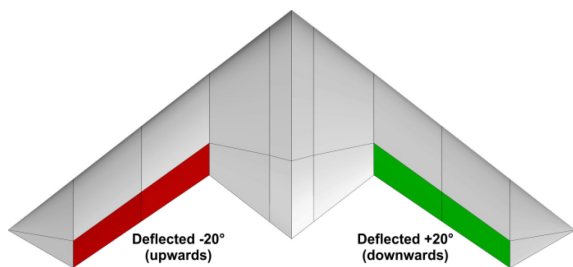


(c) Tau mesh

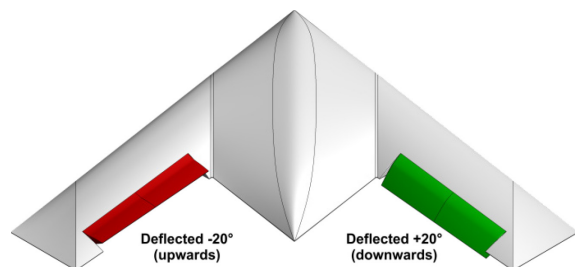


(d) DLR-F19 wind tunnel model

FIGURE 11. Aircraft models for computation and wind tunnel measurements



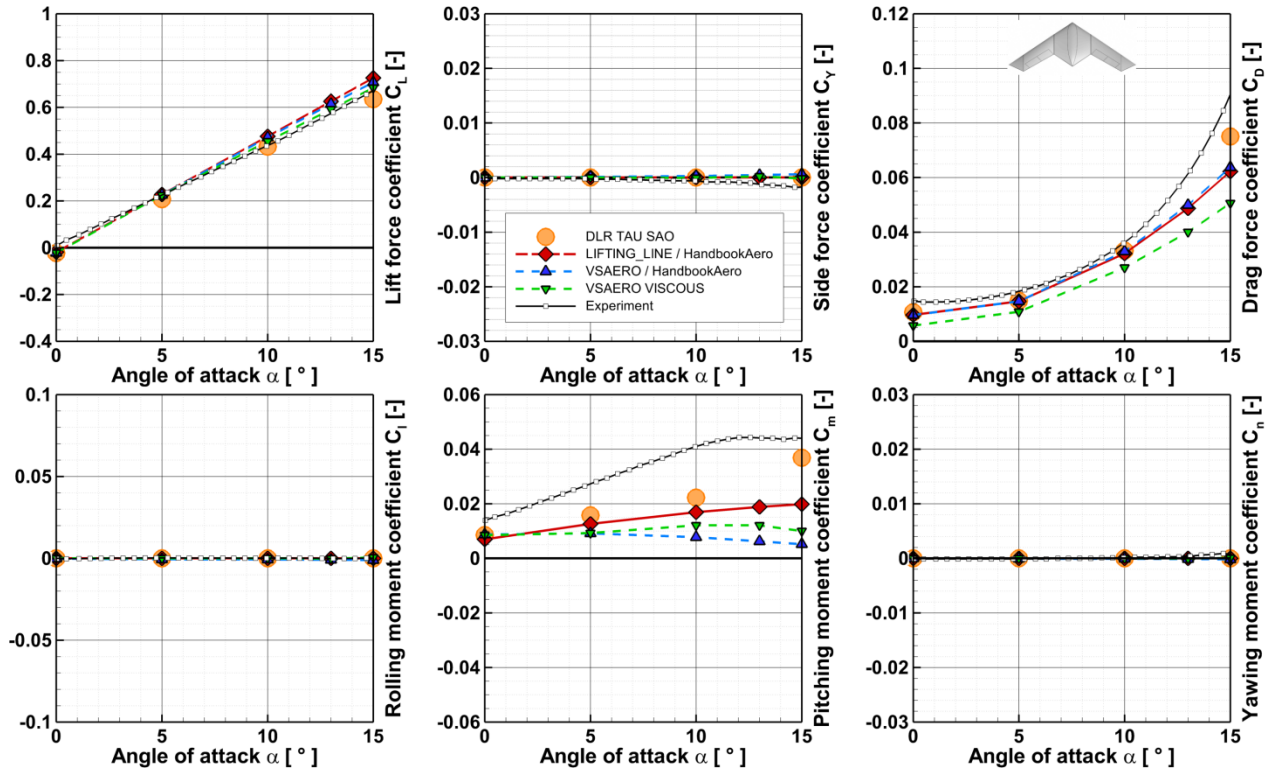
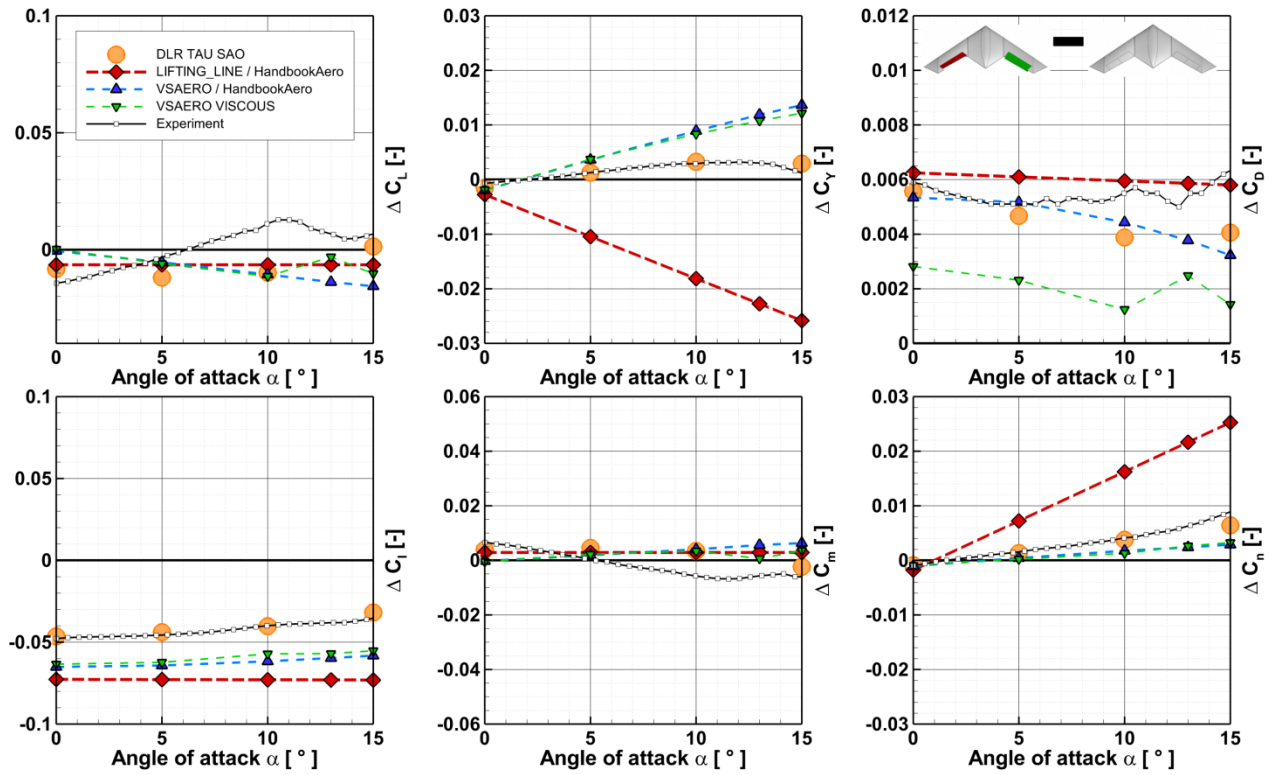
(a) LIFTING\_LINE and VSAERO

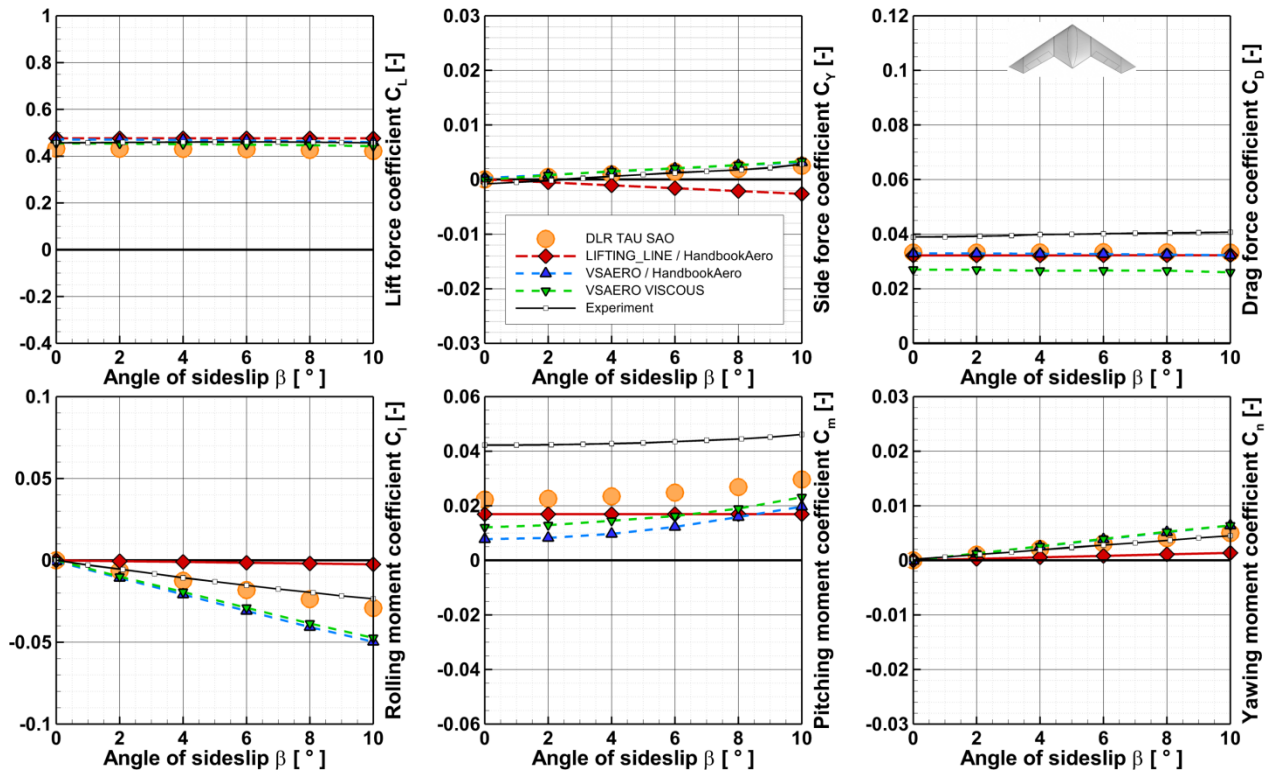
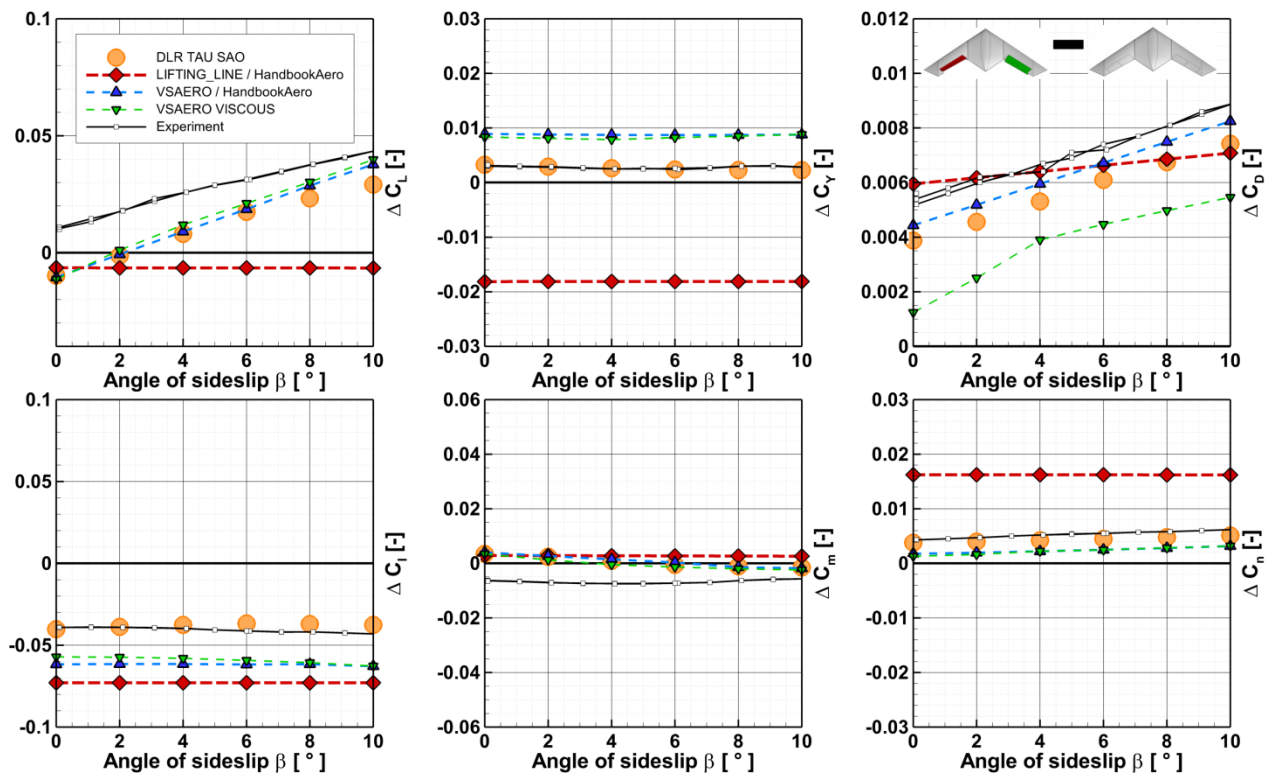


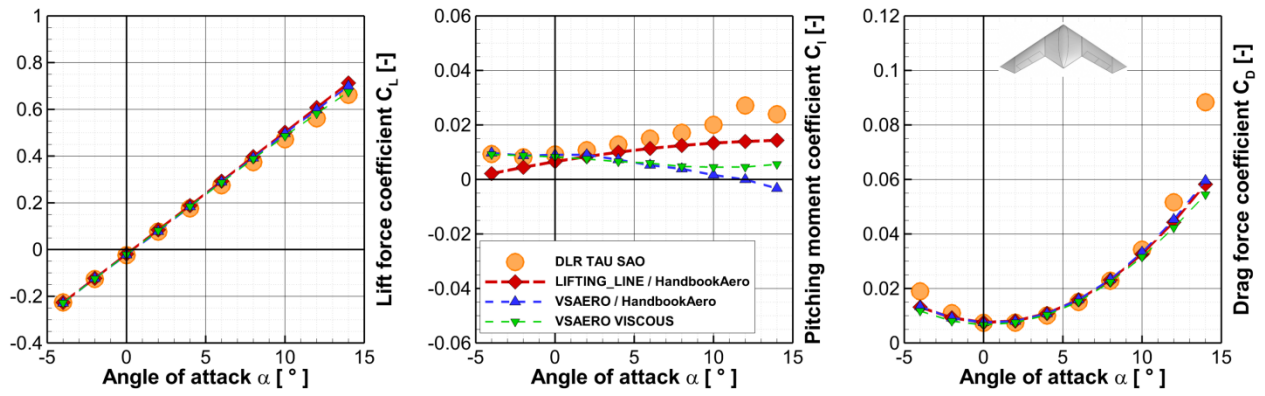
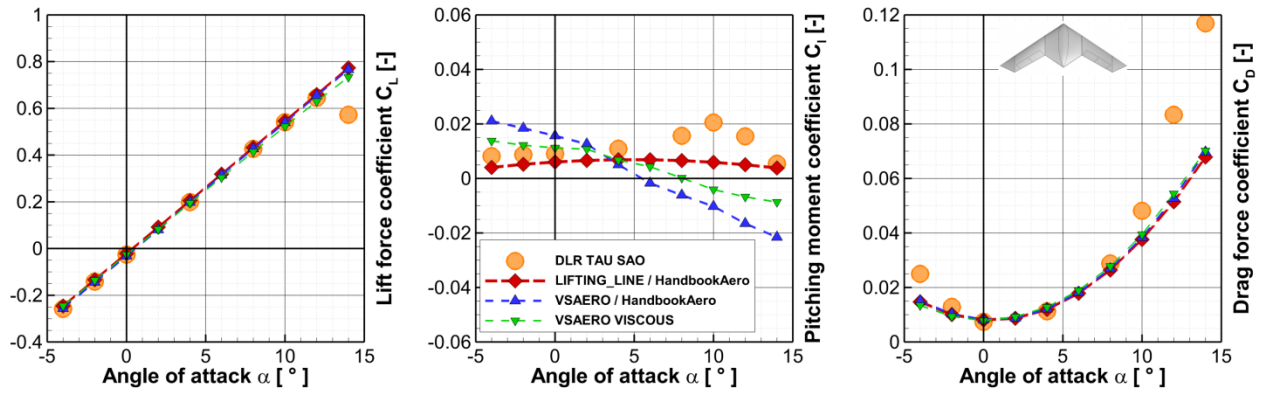
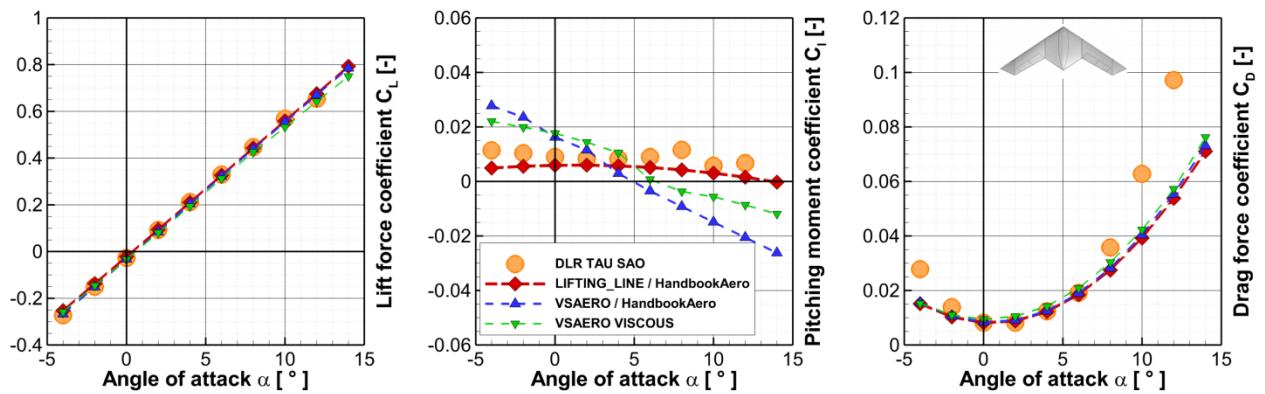
(b) Tau and wind tunnel model

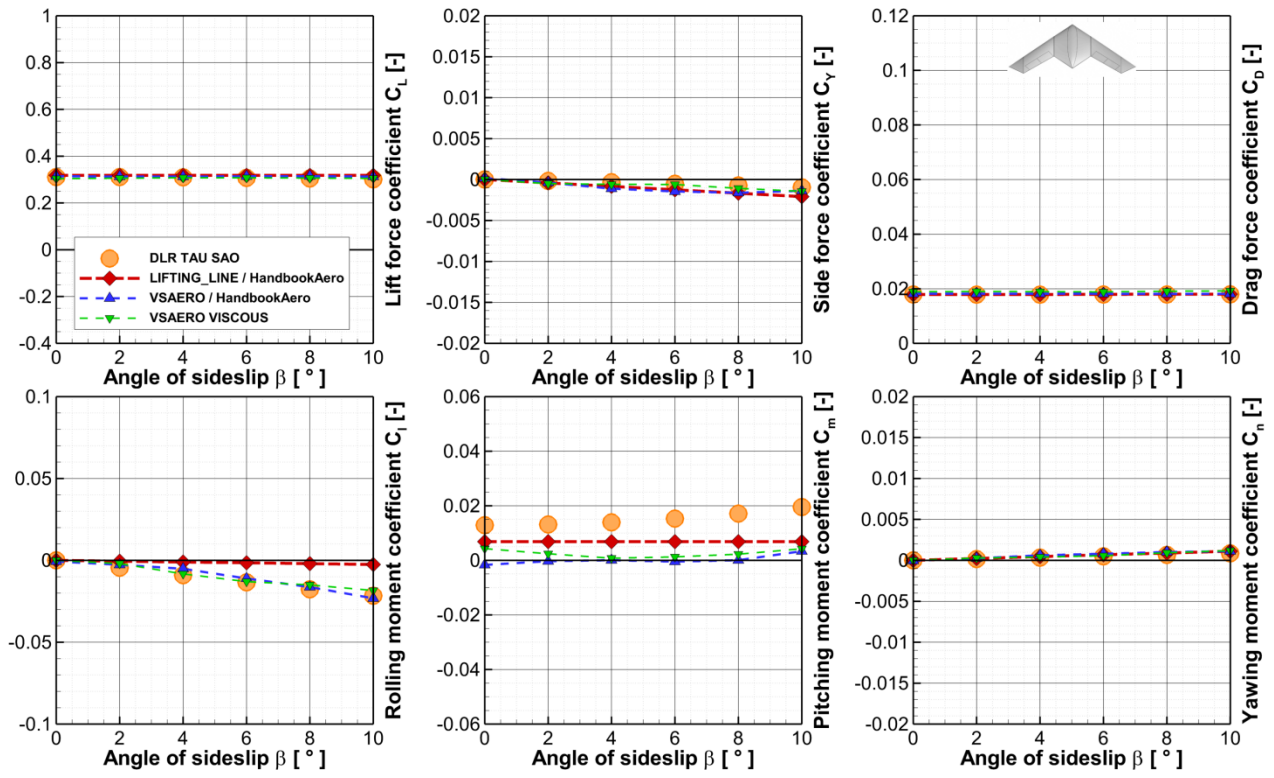
FIGURE 12. Differences in control surface geometry




 FIGURE 13. Total coefficients of clean configuration ( $M = 0.15$ ,  $RE = 1.6 \cdot 10^6$ ,  $\alpha$  variation,  $\beta = 0^\circ$ )

 FIGURE 14. Delta coefficients due to deflected inboard and outboard control surfaces ( $M = 0.15$ ,  $RE = 1.6 \cdot 10^6$ ,  $\alpha$  variation,  $\beta = 0^\circ$ )


 FIGURE 15. Total coefficients of clean configuration (M = 0.15, RE =  $1.6 \cdot 10^6$ ,  $\alpha = 10^\circ$ ,  $\beta$  variation)

 FIGURE 16. Delta coefficients due to deflected inboard and outboard control surfaces (M = 0.15, RE =  $1.6 \cdot 10^6$ ,  $\alpha = 10^\circ$ ,  $\beta$  variation)


 FIGURE 17. Total coefficients of clean configuration ( $M = 0.55$ ,  $RE = 23 \cdot 10^6$ ,  $\alpha$  variation,  $\beta = 0^\circ$ )

 FIGURE 18. Total coefficients of clean configuration ( $M = 0.80$ ,  $RE = 23 \cdot 10^6$ ,  $\alpha$  variation,  $\beta = 0^\circ$ )

 FIGURE 19. Total coefficients of clean configuration ( $M = 0.85$ ,  $RE = 23 \cdot 10^6$ ,  $\alpha$  variation,  $\beta = 0^\circ$ )

FIGURE 20. Total coefficients of clean configuration (M = 0.80, RE =  $23 \cdot 10^6$ ,  $\alpha = 6^\circ$ ,  $\beta$  variation)